Exploring fast proton transfer events associated with lateral proton diffusion on the surface of membranes

Nadav Amdursky[a,1], Yiyang Lin[b], Noora Aho[c], and Gerrit Groenhof[c]

[a]Schulich Faculty of Chemistry, Technion – Israel Institute of Technology, Haifa 3200003, Israel; [b]Department of Materials, Imperial College London, SW7 2AZ London, United Kingdom; and [c]Department of Chemistry and NanoScience Center, University of Jyväskylä, FIN-40014, Jyväskylä, Finland

Edited by Harry B. Gray, California Institute of Technology, Pasadena, CA, and approved December 19, 2018 (received for review July 18, 2018)

Proton diffusion (PD) across biological membranes is a fundamental process in many biological systems, and much experimental and theoretical effort has been employed for deciphering it. Here, we report on a spectroscopic probe, which can be tightly tethered to the membrane, for following fast (nanosecond) proton transfer events on the surface of membranes. Our probe is composed of a photoacid that serves as our light-induced proton source for the initiation of the PD process. We use our probe to follow PD, and its pH dependence, on the surface of lipid vesicles composed of a zwitterionic headgroup, a negative headgroup, a headgroup that is composed only from the negative phosphate group, or a positive headgroup without the phosphate group. We reveal that the PD kinetic parameters are highly sensitive to the nature of the lipid headgroup, ranging from a fast lateral diffusion at some membranes to the escape of protons from surface to bulk (and vice versa) at others. By referring to existing theoretical models for membrane PD, we found that while some of our results confirm the quasi-equilibrium model, other results are in line with the nonequilibrium model.

proton diffusion | excited-state proton transfer | lipid vesicles | photoacid | molecular dynamics

The translocation of protons across the two sides of biological membranes by transmembrane proteins is a fundamental biochemical process, such as the transport of protons in the aerobic respiration system in the mitochondria of eukaryotes or in the chloroplast of plants and prokaryotes during photosynthesis (1, 2). In this proton translocation process, protons arrive at the entrance of the protein-based proton pump either from the membrane or from the bulk solution. The diffusion of protons in bulk aqueous solution is highly efficient, with a diffusion coefficient (D_{H^+}) of $D_{H^+} = 9.3 \times 10^{-5}$ cm^2·s^{-1}, as commonly explained by the Grotthuss mechanism, which describes a hydrogen bond-assisted proton hopping between water molecules (3, 4). However, the diffusion of protons along the surface of the membrane toward the entrance of the pump is still under investigation. The protein structure of proton pumps suggests that a protein structural motif in the form of ionizable side chains of amino acids is responsible for shuttling the protons from the surface of the membrane to the protein pump (1, 2, 5). It was established more than 20 years ago that proton transfer (PT) from the surface of membranes to bulk water (and vice versa) is different from PT events in bulk water (6–10). Proton diffusion (PD) along a membrane surface is more complicated than bulk PD since the structure of the lipid molecule, the distance between adjacent lipid molecules, and the water molecules in and around the lipid membrane all affect PD. Due to advances in fast spectroscopy experiments and molecular dynamics (MD) simulations, significant progress in our understanding of this type of PD has been made in the past decade (11–23).

In a pioneering type of experiment, the groups of Pohl and coworkers (11–14) and Widengren and coworkers (15, 16) have explored the role of the lipid and bulk proton concentration on PD along membranes. Widengren and coworkers (15, 16) have used a fluorescent chromophore that was tethered to the membrane surface; by fluorescence correlation spectroscopy, they followed the protonation of the chromophore. Their main conclusion was that the lipids act as proton-collecting antennas from the bulk solution. They further found that (*i*) incorporating phosphatidic acid (PA) in vesicles of phosphatidylcholine (PC) or phosphatidylglycerol (PG) caused an increase in PD (16) and (*ii*) both the ionic strength of the solution and the mode of protonation of the proton-collecting antennas influence the PD parameters (15). The lateral PD coefficient on the membrane was indirectly estimated by the authors while assuming a proton hopping between adjacent lipid molecules (with a distance of 1 nm), and resulted in a diffusion coefficient of $D_{H^+} = 2 \times 10^{-7}$ cm^2·s^{-1}. Pohl and coworkers used a similar chromophore as in the latter experiments, but the release of protons was either photoinitiated from a proton release chromophore that was situated dozens of micrometers from the probed chromophore (11, 13) or by proton injection a few micrometers from the detection site (12, 23). This experimental approach can only be used with planar membranes (instead of vesicles), but it enables the direct calculation of the diffusion coefficient from the kinetic curves. The authors' main conclusions were (*i*) PD along a PC membrane was similar to the one along a phosphatidylethanolamine (PE) membrane sharing a diffusion coefficient of $\sim 4 \times 10^{-5}$ cm^2·s^{-1}; (*ii*) surprisingly, the diffusion along a glycerol monooleate (GMO) membrane was similar to the PC and PE membranes; and (*iii*) PD is most probably due to protons in the second layer of water around the membrane.

Here, we explore PD along the surface of lipid vesicles by following the light-initiated proton release from a membrane-anchored photoacid, which dissociates upon light excitation due to the large difference in pK_a value between its ground and excited states. Using time-resolved fluorescence enables us to extract the PT efficiency to and from the photoacid, the PD coefficient, and

Significance

Proton diffusion (PD) across biological membranes is a fundamental process in many biological systems, such as in aerobic respiration or in the photosynthesis process. Even though this diffusion process has been studied for many decades, it is still highly enigmatic. Here, we suggest an experimental technique to study the very fast PD events taking place upon the photoinduced release of a proton on the surface of the membrane. We show that the diffusion, as well as the interaction between protons on the surface and protons in bulk media can be influenced by the nature of the membrane's lipids. Our results shed some light on this unique PD process and help to overcome previous experimental contradictions in the literature.

Author contributions: N. Amdursky, Y.L., and G.G. designed research; N. Amdursky, Y.L., and N. Aho performed research; N. Amdursky, Y.L., N. Aho, and G.G. contributed new reagents/analytic tools; N. Amdursky, N. Aho, and G.G. analyzed data; and N. Amdursky wrote the paper.

The authors declare no conflict of interest.

This article is a PNAS Direct Submission.

[1]To whom correspondence should be addressed. Email: amdursky@technion.ac.il.

This article contains supporting information online at www.pnas.org/lookup/suppl/doi:10.1073/pnas.1812351116/-/DCSupplemental.

Published online January 24, 2019.

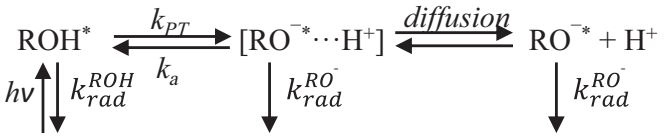

Scheme 1. ESPT photoprotolytic cycle of photoacids. *hν*, photon absorption; *rad*, radiative decay.

the dimensionality of the diffusion. We explore four types of membranes with different phospholipid headgroups: a zwitterionic headgroup (PC), a negative headgroup (PG), a headgroup that is composed only of the negative phosphate group (PA), and a positive headgroup without the phosphate group [trimethylammonium-propane (TAP)] (24). The use of photoacids to follow proton dynamics on the surface of lipid membranes started in the pioneering works of Nachliel and Gutman (25) nearly 30 years ago. In contrast to that study, in which the photoacid was solvated in solution, we have tightly tethered the photoacid to the surface of the lipid, and thus follow only protons that have been released on the surface.

Theoretical Model

Photoacids (Brønsted type) are aryl-OH molecules, whose pK_a values differ between ground and excited states. For instance, the common photoacid of 8-hydroxy-1,3,6-pyrenetrisulfonate (HPTS) has a pK_a value of 7.4 in the ground state and a pK_a* value of 1.3 in the excited state (26). Accordingly, the molecule dissociates during the excited-state lifetime, and the excited-state proton transfer (ESPT) photoprotolytic cycle can be described as follows.

Following light excitation of the protonated species (ROH), the excited molecule (ROH*) deprotonates with a PT rate of k_{PT}. The proton can then either recombine with the anion (RO^{-}*), with a recombination rate of k_a, or diffuse along the media, which can be described by the Debye–Smoluchowski equation (27). The arrows pointing down in Scheme 1 represent the radiative decay of the ROH* and RO^{-}*, which share a similar radiative lifetime, τ, of ∼5.4 ns, which enables following the PD for at least 30 ns using time-resolved experimental methods. The fluorescence intensity and decay of the ROH* and RO^{-}* forms can be easily followed individually since each form emits at a different wavelength. Photoacids have been used to follow the hydration of biological surfaces of proteins (26, 28–30) and polysaccharides (26, 31, 32). The photoprotolytic cycle of photoacids (Scheme 1) has been theoretically modeled by Agmon and coworkers (27, 33–35), who suggested the following expression for the ROH* fluorescence decay:

$$I_f^{ROH^*} * \exp\left(-t/\tau\right) \cong \frac{\pi a^2 k_a \exp[-R_D/a]}{2k_{PT}(\pi D_{H^+} t)^{d/2}}. \quad [1]$$

This model describes an ESPT process occurring on a surface of a reaction sphere with a radius of a, where d is the dimensionality of the PD and R_D is the Debye radius. In their model, R_D represents the distance at which the coulombic attraction between the negative excited-state anion (RO^{-}*) and the positive proton equals the thermal energy (k_BT):

$$R_D = \frac{|Z_1 Z_2| e^2}{4\pi\varepsilon_0 \varepsilon_r k_B T}, \quad [2]$$

where Z_1 and Z_2 are the electron charge (e) units of RO^{-}* and the dissociated proton, ε_0 is the permittivity of free space, and ε_r is the relative dielectric permittivity of the medium. The relative dielectric permittivity of the water layer surrounding the lipid vesicle is hard to estimate, and we have used an averaged value of 20–27 for the first nanometers around the lipid vesicles as was found experimentally and theoretically (36, 37). Accordingly, the calculated Debye radius for our membrane-bound modified photoacid (Scheme 2) is R_D = 20–28 Å. HPTS in solution has a fourfold higher Z_1 value (its RO^{-}* form has four electron charges), but due to the high relative dielectric permittivity of water (ε_r = 80), HPTS has a value of R_D = 28 Å.

Results

For tethering the photoacid to the surface of a lipid vesicle, we synthesized a hydrophobic photoacid where a dodecyl group has been attached to each of the sulfonate groups of HPTS (C_{12}-HPTS; Scheme 2). Due to the hydrophobic nature of our newly synthesized photoacid, it could not be dissolved in water. Comparing the steady-state emission of HPTS and C_{12}-HPTS in ethanol and methanol has allowed us to conclude that C_{12}-HPTS can be considered as a stronger photoacid than HPTS (*SI Appendix*, Fig. S1 and further discussion). A stronger photoacid is more likely to undergo ESPT. Our finding is in line with the works of Jung and coworkers (38, 39), who observed an increase in the photoacid strength upon modifications of the HPTS sulfonic groups.

C_{12}-HPTS was tethered to the membrane (at a ratio of 1:100 probe/lipid; *Materials and Methods*), which was composed of the following lipids: 1-palmitoyl-2-oleoyl-*sn*-glycero-3-phospho-1′-*rac*-glycerol (POPG), 1-palmitoyl-2-oleoyl-*sn*-glycero-3-phosphocholine (POPC), 1-palmitoyl-2-oleoyl-*sn*-glycero-3-phosphate (POPA), or 1,2-dioleoyl-3-trimethylammonium-propane (DOTAP). We have used dynamic light scattering to quantify the size distribution of the different formed vesicles, showing similar distribution of our different vesicles (*SI Appendix*, Fig. S2).

MD Study. Our working hypothesis here is that our newly designed probe can integrate into the membrane while exposing its hydroxy group toward the membrane surface (i.e., in the water membrane interface) and release a proton upon light irradiation. To test this hypothesis, we performed atomistic MD simulations of the C_{12}-HPTS incorporated in lipid bilayers of POPC, POPG, and POPA. The incorporation in DOTAP vesicles was not simulated since, as will be discussed below, ESPT from C_{12}-HPTS in

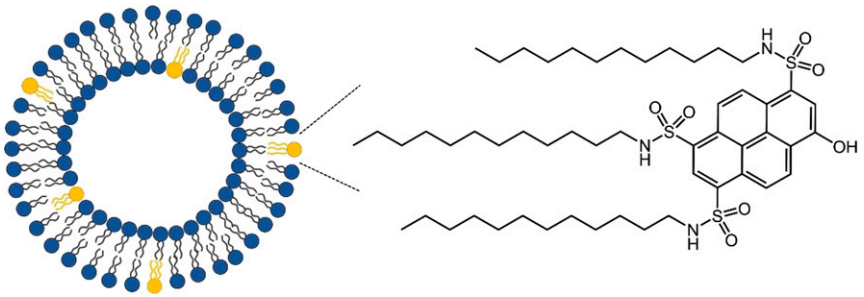

Scheme 2. Molecular scheme of C_{12}-HPTS incorporated into a lipid vesicle.

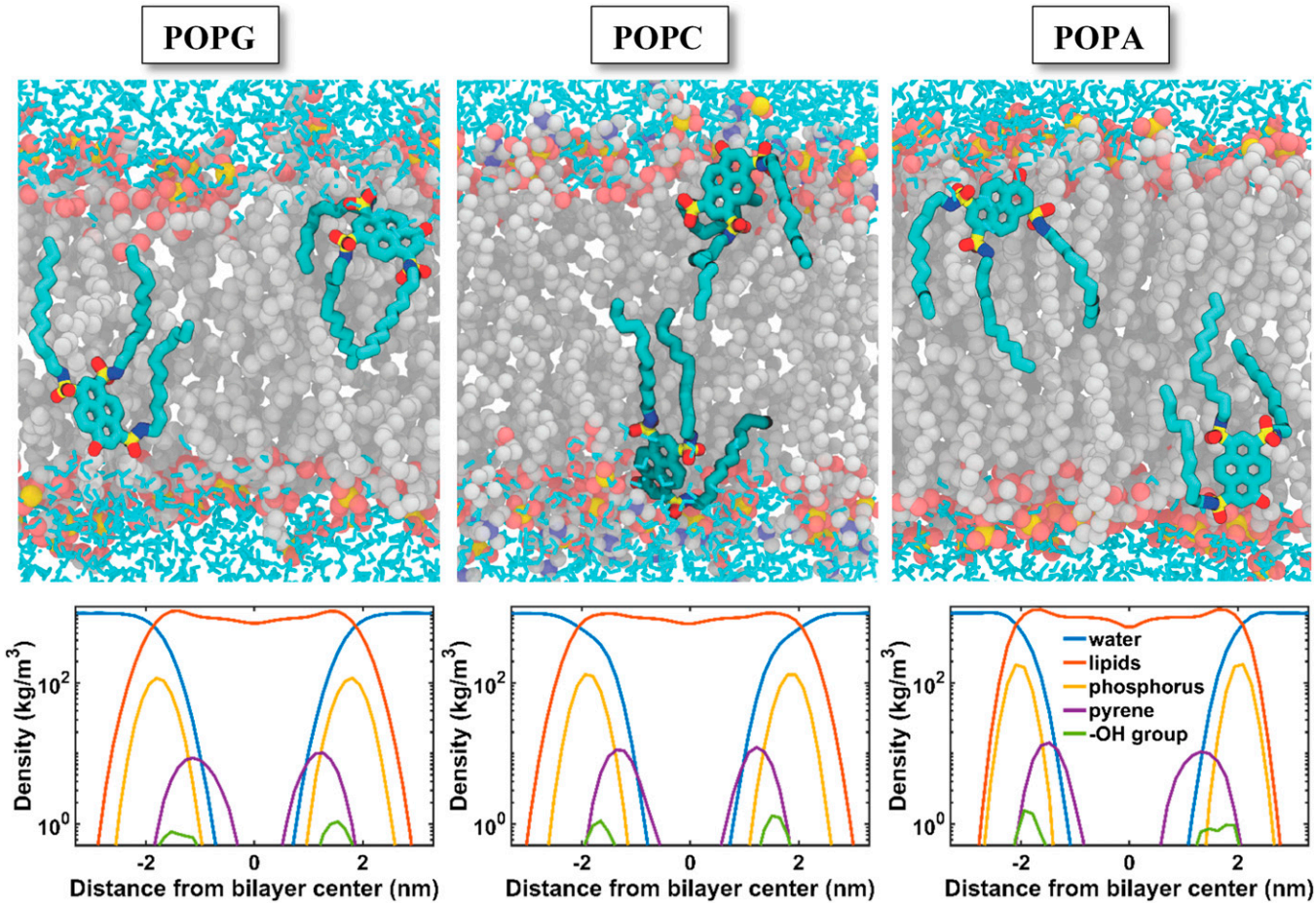

Fig. 1. (*Top*) Snapshots from atomistic MD trajectories showing the position of the C_{12}-HPTS dye in the upper and lower leaflets of the three phospholipid bilayers (water molecules are shown as cyan sticks). (*Bottom*) Density distributions along the bilayer normal of the water (blue), lipids (red), phosphorus atoms of the lipid headgroups (yellow), C_{12}-HPTS pyrene moieties (violet), and C_{12}-HPTS hydroxy groups (green).

DOTAP could not be followed in physiological aqueous conditions. The molecular snapshots of the MD simulations (Fig. 1, *Top*) show that C_{12}-HPTS is well integrated within the membrane, exposing its −OH toward the water–membrane interface, in close proximity to the location of the phosphate groups, as can be observed in the density plots (Fig. 1, *Bottom*). The MD simulations also allowed us to estimate whether the −OH of the photoacid can release a proton by following the ability of the photoacid's hydroxy group to form hydrogen bonds with nearby water molecules or phosphate groups (Table 1). The table shows that the −OH can form hydrogen bonds with nearby moieties for the vast majority of the simulation time. Furthermore, the ratio between the number of hydrogen bonds to water molecules and the number of hydrogen bonds to nearby phosphate groups depends on lipid, with the maximum number of hydrogen bonds to water for the POPA membrane. As will be discussed later (see *Discussion*), these results support our spectroscopic measurements.

Steady-State Spectroscopy. Steady-state absorption (Fig. 2) studies of the photoacid-containing lipid vesicles allowed us to verify that C_{12}-HPTS has been tethered to the membrane and to determine the pK_a of the photoacid by ratiometric titration with a strong acid/base. Fig. 2 and Table 2 show that the pK_a of the photoacid is highly sensitive to the charge of the lipid headgroup (molecular schemes in Fig. 2). We found that the pK_a in the negatively charged headgroup vesicles (POPG and POPA) is higher than in the zwitterionic headgroup vesicle (POPC), while the pK_a in the positively charged headgroup vesicles (DOTAP) is extremely low. It has been shown that the pK_a of HPTS in aqueous solutions can be changed as a function of salt concentration (40) at different water/organic solvent ratios (41) or next to a protein surface (30),

Table 1. Percentage of time that a hydrogen bond is formed between the −OH group of C_{12}-HPTS and the surrounding water molecules or lipid phosphate groups

Lipid system	Hydrogen bonds with water molecules, %	Hydrogen bonds with lipid phosphates, %	Total hydrogen bonds with everything, %
POPG	31.9	65.9	97.8
POPC	27.1	71.3	98.4
POPA	37.4	56.2	93.6

The values are averaged between the upper and lower membrane leaflets in the MD simulations.

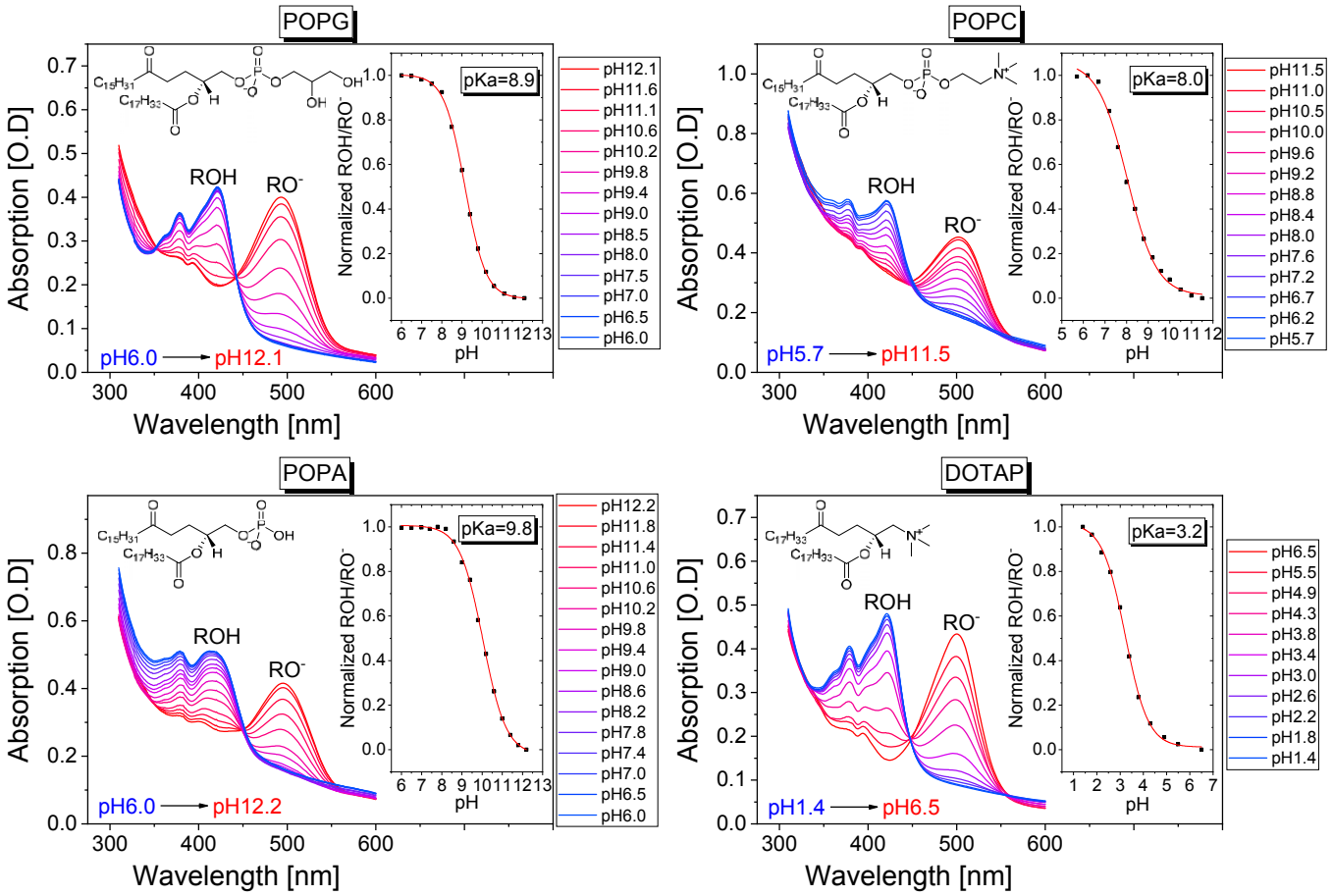

Fig. 2. Absorption spectrum of C_{12}-HPTS incorporated in the different lipid vesicles at different pH values. (*Insets*) pK_a calculations and the molecular schemes of the lipid. O.D, optical density.

but, as far as we are aware, such drastic change in the pK_a value of a given photoacid has never been observed before. Our latter finding further suggests that the photoacid is in tight proximity to the headgroup of the lipid, in line with the results from our MD simulation. In a similar manner, Widengren and coworkers (15) also observed an increase in the pK_a values of fluorescein and Oregon green when these photoacids were tethered to PG and PC vesicles. We have used the absorption and emission maxima (Table 2) to calculate the ΔpK_a values ($\Delta pK_a = pK_a - pK_a^*$) of the photoacid at different lipid vesicles using the Förster cycle (42):

$$\Delta pK_a = \frac{\Delta E}{\ln(10)RT}, \qquad [3]$$

where ΔE is the energy difference between the protonated (ROH) and deprotonated (RO^-) forms of the photoacid, R is the gas constant, and T is temperature. To calculate ΔE, we have used the averaged values for the absorption (E_{Ab}) and emission (E_{Em}) maxima to compensate the solvent contribution to the Stokes' shifts (43):

$$\Delta E = \left(E_{Ab}^{ROH} + E_{Em}^{ROH}\right)/2 - \left(E_{Ab}^{RO^-} + E_{Em}^{RO^-}\right)/2. \qquad [4]$$

For following the light-induced proton release from photoacids, they have to be excited in their ROH form. Accordingly, the above-calculated pK_a values limit the pH range of the measurement, in which only low pH values could be used for DOTAP vesicles. Fig. 3 shows the normalized emission spectrum with different lipid vesicles and at different pH values, where several important observations can be made. The first one is that for all of our measurements, the main form of the molecule is RO^-, meaning that the photoacid can dissociate and release a proton. This is a further validation that the photoacid is on the surface of the lipid vesicle, since if it were buried within the hydrophobic membrane, we would expect to see the ROH peak as the main one, as was previously shown for HPTS within hydrophobic binding sites (26).

The second important observation is that the emission profile is different for different lipid vesicles, which indicates that the lipid headgroup has a major role in determining the ESPT parameters of the photoprotolytic cycle of C_{12}-HPTS (Scheme 1). We can use the RO^-/ROH ratio of the emission spectrum at different pH values (*SI Appendix*, Table S1) as a first indication for the role of the lipid headgroup in ESPT to/from the photoacid and for PD. In general, high RO^-/ROH ratios (low-intensity ROH peak; Fig. 3) can be a result of a fast PT rate, a slow recombination rate, or a fast PD

Table 2. Absorption and emission maxima of ROH and RO^-, together with the calculated pK_a, ΔpK_a, and pK_a^* values

System	POPG	POPC	POPA	DOTAP
λ_{abs}^{ROH}, nm	419	420	411	422
$\lambda_{abs}^{RO^-}$, nm	501	502	500	501
λ_{em}^{ROH}, nm	475	476	473	459
$\lambda_{em}^{RO^-}$, nm	543	543	541	544
pK_a	8.9	8.0	9.8	3.2
ΔpK_a	7.0	6.9	7.5	7.6
p$K_a^{*\dagger}$	1.9	1.1	2.3	−4.4

†The values were estimated by $pK_a^* = pK_a - \Delta pK_a$.

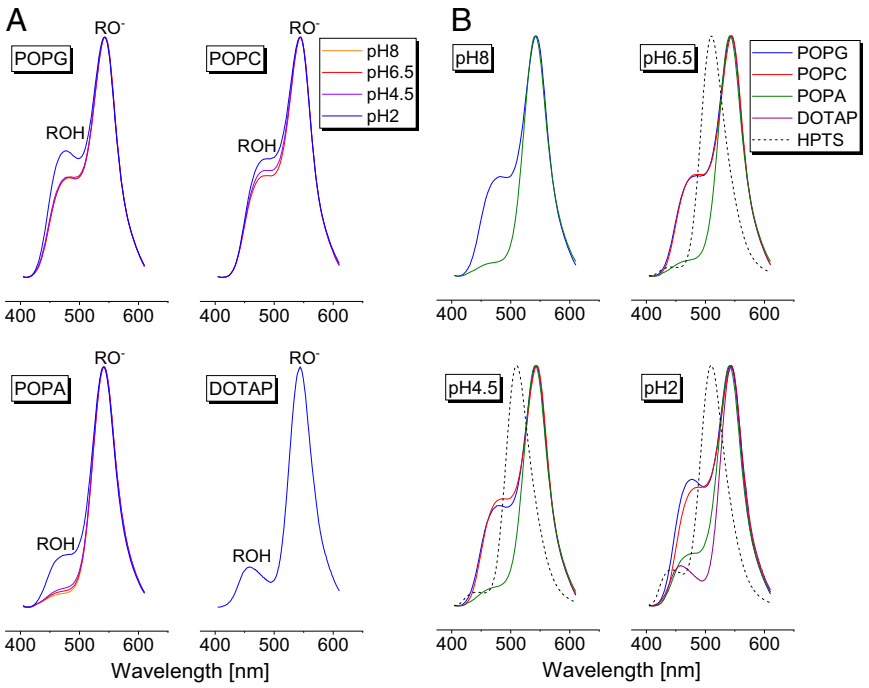

Fig. 3. Emission spectrum of C_{12}-HPTS incorporated in the different lipid vesicles at different pH values, below the pK_a of the photoacid. (*A*) Spectrum for each of the lipid vesicles as a function of pH. (*B*) Spectrum at each of the pH values as a function of the lipid vesicle. The dashed lines in *B* represent the emission spectrum of HPTS.

coefficient, and vice versa, while only with transient fluorescence can we distinguish between them (*vide infra*). The RO^-/ROH ratio and the emission peak positions of C_{12}-HPTS in POPC and POPG are very similar. This means that although the surface charge is different (POPG is negatively charged, while POPC is zwitterionic), the ESPT parameters on their surface are similar. The higher RO^-/ROH ratios of the less bulky POPA (negatively charged) and DOTAP (positively charged) lipid vesicles imply some role of the lipid headgroup bulkiness in PD; however, as will be discussed below (see *Discussion*), the cause for it is very different.

Time-Resolved Fluorescence. Following our steady-state measurements that confirmed the ability of C_{12}-HPTS to release a proton, and already suggested that PD is different on the surface of lipid vesicles composed of different headgroups, we have turned to time-resolved fluorescence measurements. Figs. 4 and 5 show the fluorescence time-resolved decay of the ROH* form at different lipid vesicles and at different pH values, respectively, in comparison to the decay of HPTS (the decay of HPTS at different pH values is shown in *SI Appendix*, Fig. S3). Qualitatively, we can divide the decay profile of ROH* into three components (Table 3), where the first fast component is directly related to the PT from the photoacid (k_{PT}), which takes place in the first nanosecond, and the other slower components are indicative of the PD and the recombination rate (k_a). Following PT, the proton can either diffuse or recombine with the RO^{-*} (Scheme 1), where the PD efficiency and dimensionality influence mainly the 1- to 6-ns regime after excitation, and the recombination can be associated with a long-lived (high-intensity) exponential tail that can span to tens of nanoseconds (27, 34). This qualitative understanding of the ROH* decay profile can be nicely explained by referring to free HPTS in solution at different pH values (Table 3 and *SI Appendix*, Fig. S3 and text within). Accordingly, we can divide the decay profile of C_{12}-HPTS (Figs. 4 and 5 and Table 3) into three different profiles:

i) The decays of POPG and POPC have a similar shape and around the same intensities, with a much slower k_{PT} (τ_1) compared with HPTS in bulk solution (Fig. 5), and their change in decay as a function of pH (both τ_{1-3} and a_{1-3}) is relatively moderate (Fig. 4).

ii) The decay of POPA is very different from that of POPG and POPC, but it has some resemblance to HPTS, both in its fast k_{PT} (τ_1) and especially in the presence and magnitude of the exponential long-lived fluorescent tail (a_3 and τ_3) at low pH.

iii) DOTAP, with its single measurement at low pH, has a unique decay profile, different from all other measurements, with a τ_1 between the ones of POPA and POPC/POPG and a relatively "small" long-lived fluorescent tail (τ_3).

For trying to quantify the different PT rate constants, diffusion coefficient, and dimensionality of the PD, we have used the above theoretical approach, utilizing a software package developed by Krissinel and Agmon (44) for solving diffusion problems, and specifically ESPT from photoacids [spherical symmetric diffusion problem (SSDP) program, version 2.66]. Since the model was not designed for highly concentrated proton solutions (low pH), manifested as a high-intensity, long-lived exponential fluorescent tail (as discussed above), we have used it only for the results obtained at pH 6.5, and thus did not fit the decay obtained with the DOTAP vesicles (fits are displayed in *SI Appendix*, Fig. S4). Below, we summarize our results (Table 4):

i) The PT rate constant, k_{PT}, on the surface of all lipid vesicles is lower than the one for HPTS in bulk water, whereas the value for POPA is the highest among all other vesicles.

ii) The proton recombination rate constant, k_a, for POPG and POPC is much higher than the one for HPTS in water, while the one for POPA is closer to the one of HPTS.

iii) The PD coefficient (D_{H^+}) from the photoacid on the lipid vesicles is reduced from the high proton mobility in bulk water and has different values for different lipid vesicles. POPA exhibits a very close value to HPTS, and POPG and POPC have a similar lower coefficient.

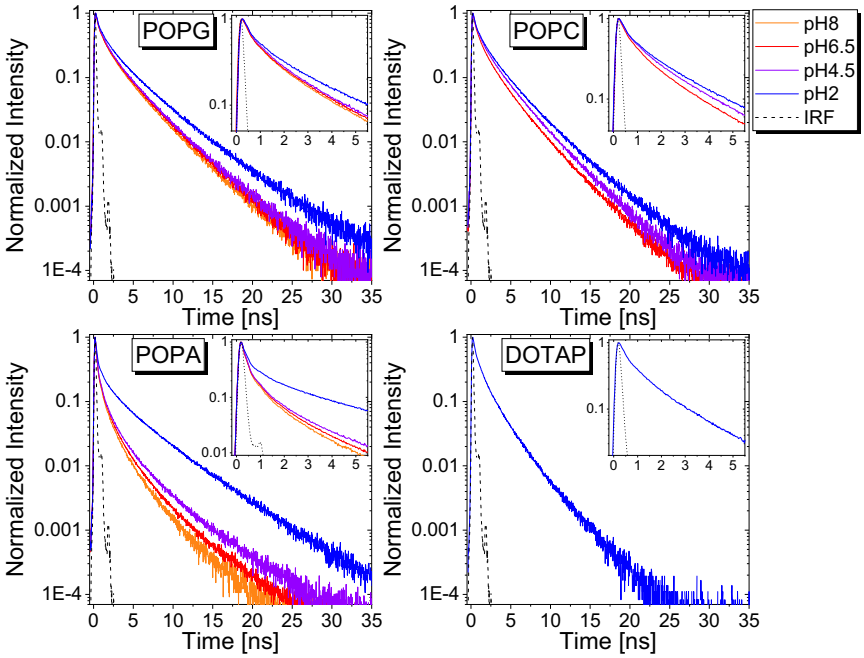

Fig. 4. Time-resolved fluorescence decay of the ROH* form in the four lipid vesicles as a function of pH value. (*Insets*) Zoomed-in views of the first nanoseconds. IRF, instrument response function.

iv) The dimensionality (d) of the PD from the photoacid on the lipid vesicles is reduced from the dimensionality value of 3 of HPTS in bulk water. POPC and POPG have a dimensionality value of 2, and POPA has a higher dimensionality value of 2.5.

v) The R_D values differ between different lipid vesicles, indicating that the dielectric constant next to the lipid vesicle changes for different lipid headgroups.

Discussion

According to the time-resolved fluorescence measurements and their fitting, we can divide the PD behavior into three different types of diffusion patterns.

The first one relates to the surfaces of POPC and POPG, which, despite a different surface charge, share the same PT and PD properties. They both exhibit lateral (2D) PD on the surface of the membrane, with a coefficient of 3.5×10^{-5} cm^2·s^{-1}, nearly

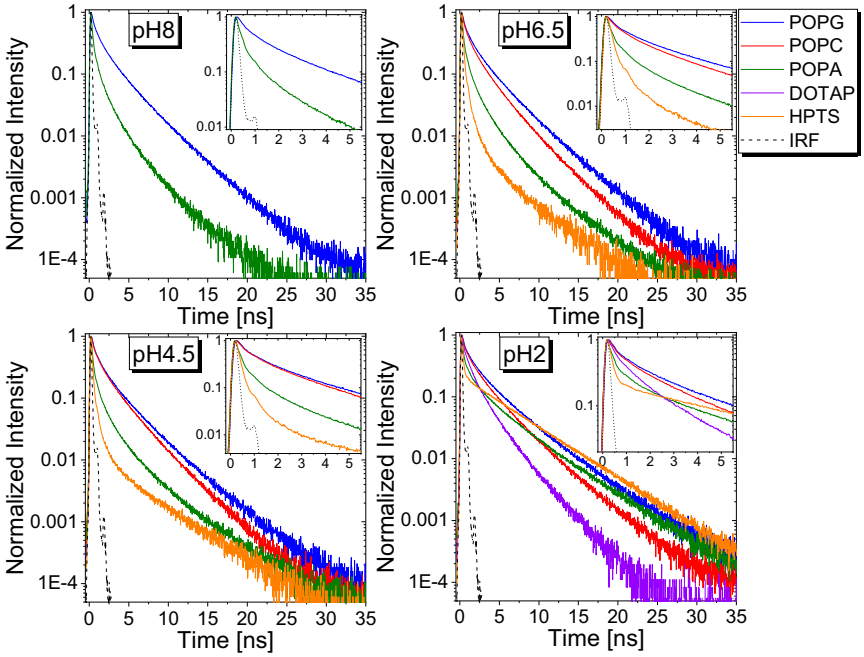

Fig. 5. Time-resolved fluorescence decay of the ROH* form at each of the pH values as a function of the lipid vesicle, in comparison to the decay of HPTS. (*Insets*) Zoomed-in views of the first nanoseconds. IRF, instrument response function.

Table 3. Fitting parameters of a three-exponent decay function for C_{12}-HPTS fluorescence in different lipid vesicles and at different pH values and for HPTS

System	pH	a_1	τ_1, ns	a_2	τ_2, ns	a_3	τ_3, ns
POPG	8.0	0.45	0.42	0.37	1.48	0.18	3.14
	6.5	0.47	0.46	0.35	1.55	0.18	3.25
	4.5	0.45	0.45	0.36	1.55	0.19	3.25
	2.0	0.43	0.51	0.36	1.77	0.21	3.78
POPC	6.5	0.46	0.41	0.38	1.34	0.16	2.88
	4.5	0.43	0.40	0.38	1.51	0.19	2.93
	2.0	0.44	0.42	0.36	1.67	0.20	3.21
POPA	8.0	0.70	0.14	0.26	0.86	0.04	2.58
	6.5	0.69	0.14	0.26	0.88	0.05	2.76
	4.5	0.69	0.15	0.26	0.93	0.05	3.16
	2.0	0.59	0.16	0.27	1.48	0.14	4.22
DOTAP	2.0	0.52	0.36	0.35	1.24	0.13	2.52
HPTS	6.5	0.82	0.13	0.17	0.55	0.006	3.55
	4.5	0.82	0.14	0.17	0.57	0.006	4.14
	2.0	0.72	0.13	0.15	2.53	0.13	5.21

The preexponential factors (a) have been normalized to $a_1 + a_2 + a_3 = 1$.

threefold slower than the one for protons in bulk water. The PT from the photoacid on the surface of these vesicles is also slower, with a k_{PT} that is more than threefold lower than the one of HPTS in bulk water (also τ_1 in Table 3). The k_a value for these lipid surfaces is around twofold larger than the one of HPTS (also τ_3 in Table 3). The high proton recombination rate on the surface of POPC and POPG can be explained by the constrained lateral PD that increases the possibility for a recombination event between a proton and the excited anion species (RO^{-*}). Interestingly, while τ_3 and its magnitude (a_3) are only weakly influenced by the pH of the solution, they change dramatically for HPTS in bulk water. This indicates a limited influence of bulk protons on the PD properties of these membranes.

The second pattern is observed for the negatively charged surface of POPA. The PD from the photoacid exhibits a mixed dimensionality of ~2.5, meaning that unlike the surfaces of POPG and POPC, the protons on the surface of POPA do not diffuse laterally, but also escape to bulk water. Indeed, all of the parameters for POPA have intermediate values between the ones for HPTS in bulk water and the ones obtained for POPC and POPG. POPA has the largest PD coefficient, the fastest PT rate, and the slowest recombination rate among the three lipids (at pH 6.5). Also, the change in the long-lived fluorescent tail magnitude (τ_3 and especially a_3) is strongly modulated by the pH, similar to HPTS, which suggests that the tethered photoacid in POPA vesicles is much more exposed to bulk solution than in the other lipid vesicles. This is in line with the results of the MD simulations, which also suggest that the photoacid's hydroxy group is more solvent-exposed in POPA than in POPG or POPC (Table 1).

The third pattern relates to the positively charged surface of DOTAP. Due to the very low pK_a of C_{12}-HPTS in DOTAP, we could measure its ESPT only at a very low pH value. The main conclusion is the relative absence of the long-lived fluorescent tail (τ_3) and the relatively slow PT (τ_1). This type of pattern is common in photoacids within binding sites of proteins (28, 45), which might imply that the hydration next to DOTAP vesicles is restricted (more hydrophobic) compared to the other vesicles.

Finally, we will try to correlate our study to previous results and available PD mechanisms. Membrane PD can be followed for different time regimes depending on what experimental approach is used. Pohl and coworkers (11–14) probed PD on the millisecond-second regime, while Widengren and coworkers (15, 16) focused on the microsecond-millisecond regime. Accordingly, our results complement the fast time regime for PD, where we focus on fast nanosecond diffusion processes. Nevertheless, our results share some similarities with the slower type of measurements and can help in resolving the discrepancies in the literature. Widengren and coworkers (15, 16) followed the protonation of a lipid-tethered dye, which bears some resemblance to our approach. They found that PT on the surface of DOPG and DOPC vesicles is faster than proton exchange between surface and bulk water. This finding is in line with the high recombination rates on the surfaces of POPG and POPC observed in our work. They further found that the addition of DOPA (to DOPG vesicles) increases the protonation of their chromophore, particularly at low pH. Our observation that POPA is highly accessible to protons in solution partially supports this finding. Nevertheless, one of their main conclusions is that the surface of the membrane acts as a proton-collecting antenna, which is not supported by our measurements for POPG, POPC, and DOTAP, but can be considered compatible with our POPA results. Moreover, led by that conclusion, they estimated a low PD coefficient ($\sim 10^{-7}$ cm^2·s^{-1}) based on the distance between titratable groups in the lipid structure. According to our measurements, which enable us to estimate the diffusion coefficient directly from the data, this low value should be revised. Pohl and coworkers (11, 13) have used a similar chromophore as the latter studies, but their conclusion was different. Their experimental setup allowed them to calculate the PD coefficient directly from their kinetic curves, where they showed that all of the different membranes they used, namely, PC, PE, and GMO, shared the same diffusion coefficient on the order of 5×10^{-5} cm^2·s^{-1}. This latter value is of the same magnitude as our derived values, even though we followed PD on the nanosecond scale, while Pohl and coworkers (11, 13) followed diffusion on the millisecond-second regime. Because the GMO membrane shares the same glycerol termination as PG membranes, the similarity in the diffusion parameters in their work can be nicely correlated to our finding of similar diffusion parameters between POPC and POPG. They concluded that PT on the membrane surface cannot involve proton hopping between titratable groups. More recently, they suggested that proton wires on the surface of the membrane can facilitate PT (13). Our results confirm that PD across POPG and POPC cannot be explained by proton hopping across titratable groups, but we do show that POPA vesicles can act as proton-collecting antennas, while DOTAP vesicles cannot support high PD.

Two main PD mechanisms have been proposed to explain the membrane PD process (13, 18, 21, 46, 47). The first mechanism suggested by Medvedev and Stuchebrukhov (18, 21, 47) discusses the coupling between bulk diffusion and surface diffusion. They claim that protons can go from bulk to surface (the "antenna effect," where protons populate titratable groups) with a rate constant of k_{on}, and from surface to bulk with a rate constant of k_{off}. They further distinguish between two regimes, the slow- and

Table 4. Summary of the PT kinetic parameters (k_{PT} and k_a), proton diffusion coefficient (D_{H^+}), dimensionality (d), and R_D for C_{12}-HPTS in different lipid vesicles (at pH 6.5) as obtained using the SSDP program

System	k_{PT}, ns^{-1}	k_a, Å·ns^{-1}	D_{H^+}, cm^2·s^{-1}	d	R_D, Å
POPG	2.6	18.5	3.5×10^{-5}	2.0	20
POPC	2.8	17.0	3.5×10^{-5}	2.0	21
POPA	5.5	11.2	8.5×10^{-5}	2.5	26
HPTS	8.9	8.5	9.0×10^{-5}	3.0	28

To limit the degrees of flexibility of this model, we have fixed the value for the radius of the reaction sphere, a, to 6 nm for all fittings, which is a common value for the HPTS photoacid. τ (Eq. **1**) was set to 5.4 ns for HPTS and to 5.7 ns for C_{12}-HPTS, as determined from our lifetime measurements. SSDP, spherical symmetric diffusion problem.

fast-exchange regimes, which refer to the rate of proton exchange between surface and bulk. They suggest that the fast regime is the most probable one, and that long-distance PD processes that take place on the millisecond-second time scale can be explained by numerous k_{on}/k_{off} events that lead to a quasi-equilibrium state between surface and bulk protons. The second mechanism proposed by Agmon and coworkers (13) and Agmon and Gutman (46) suggests that protons on the surface are not in equilibrium with bulk protons. They further propose that the membrane is not acting as a proton-collecting antenna and that protons do not escape from surface to bulk (i.e., protons have very low k_{off} values). They suggest that protons on the surface diffuse via proton wires in what they envision as a propagation of an advancing front of protons, where protons at the front protonate all possible titratable sites, and that the protons following that front diffuse in an unhindered fashion. Both theories have been developed to explain results observed in the (sub)second regime. Our measurements follow only diffusion events taking place in the excited state and, accordingly, are limited to the nanosecond regime. Nevertheless, we believe that our results can shed insights on the possible fast kinetics of this diffusion process.

As discussed, our results with POPA vesicles are very different from the ones of POPC and POPG. The strong influence of the solution pH on the kinetic parameters observed for the POPA vesicles suggests that protons released on the surface of the membrane can escape to bulk, and that during the excited-state lifetime, protons from the bulk can go to the surface, which supports the quasi-equilibrium model. It is important, however, to mention that PA lipids are frequently referred to as "buffered lipids" (i.e., due to their bare phosphate group, they act as buffer molecules in solution, and can therefore be easily titratable). On the other hand, our POPC and POPG results suggest PD with limited surface-to-bulk and bulk-to-surface PT events, which, in combination with a relatively high PD coefficient, support the nonequilibrium model, as well as disproving the possibility of diffusion by proton hopping between titratable groups (11). Nevertheless, since we observed some pH dependency of the kinetic parameters, the protons cannot be completely nonequilibrated with the solution, and there is probably some bulk-to-surface PT. Thus, while our results seem to support the nonequilibrium model, we cannot ascribe all of our results to a single suggested PD mechanism, but hope that our results will ignite new theoretical efforts toward a unifying approach for PD on the surface of membranes.

Conclusions

In summary, we have developed a photoacid-based probe that can be tethered to membranes for studying light-induced PD processes on the surface of membranes. While the photoacid enables the exploration of fast PT events within the PD process, the time interval in which PD can be studied is limited to the excited-state lifetime of the probe, which is on the order of a few dozen nanoseconds. As a consequence, the accessible length scales are also limited to few dozen nanometers (48). We used our photoacid probe to explore PD across phospholipid membranes with different lipid headgroups, namely, PA, PC, PG, and TAP, as well as the effect of pH on the PD process. We found that protons diffuse laterally on the surface of PC and PG vesicles with a diffusion coefficient of 3.5×10^{-5} $cm^2 \cdot s^{-1}$, which cannot be explained by proton hopping between titratable groups, with only a moderate pH dependence on the kinetic parameters. For PA vesicles, we found that protons could escape to bulk, and vice versa (the antenna effect), which also leads to a more prominent effect of the solution pH on the kinetic parameters. For TAP vesicles, we found a slower PT from the photoacid with little influence of bulk protons, which resembles the behavior of hydrophobic pockets.

Materials and Methods

Synthesis of C_{12}-HPTS Derivative. To a mixture of dodecanamine (0.5 mmol) and triethanolamine (0.5 mmol) in 10 mL of dichloromethane (0 °C), 0.1 mmol of 8-acetoxypyrene-1,3,6-trisulfonyl chloride (38) in 10 mL of dichloromethane was added dropwise. After warming to room temperature, the reaction mixture was stirred for another 48 h. The organic phase was washed with sodium bicarbonate and saturated sodium chloride solution before being dried over sodium sulfate. After evaporation, the crude product was purified via column chromatography (3:7 ethyl acetate/petrol ether). The product was confirmed by MALDI-TOF.

Preparation of Lipid Vesicles. All lipids (POPA, POPC, POPG, and DOTAP) were purchased from Avanti Polar Lipids, Inc. The lipid was mixed with the C_{12}-HPTS probe in chloroform at a 100:1 (lipid/probe) molar ratio. The mixture was dried under a stream of N_2 and placed under vacuum for at least 2 h to remove any residual solvent. The dried lipid film was then rehydrated in 5.0 mM phosphate buffer and vortexed for 30 s. The resulting solution was extruded 31 times through a polycarbonate membrane with 200-nm pores (0.2 μm; Nucleopore). The liposome solution was diluted to a lipid concentration of 1.0 mg/mL and stored at 4 °C. Before later use, the pH of the solution was adjusted using either HCl or NaOH.

Spectroscopic Measurements. The above-mentioned lipid vesicle solutions or a 35-μM HPTS solution was used for the spectroscopic measurements. Dynamic light scattering measurements were recorded with a Malvern Zetasizer using a 1-cm-pathlength cuvette. The UV-visible absorption measurements were recorded with a PerkinElmer spectrometer using a 1-cm-pathlength quartz cuvette. The steady-state fluorescence measurements were recorded with a Horiba Fluorolog system using an excitation wavelength of 395 nm with 1-nm bandpass slits for both entrance (excitation) and exit (emission). The time-resolved fluorescence measurements were acquired with a Horiba Deltaflex system, using a 405-nm diode laser with a pulse duration of <100 ps as the light excitation source. The ROH fluorescent decay was collected at 445 nm and 455 nm for HPTS and C_{12}-HPTS, respectively, where at least 30,000 counts (at peak) were collected. The instrument response function was collected at the excitation wavelength using a diluted Ludox solution in water.

MD Simulations. Details of MD experiments are given in *SI Appendix*.

ACKNOWLEDGMENTS. We thank D. Huppert and N. Agmon for fruitful discussions. G.G. and N. Aho thank the CSC – IT Center for Science (Espoo, Finland) for computational resources. N. Amdursky received financial support from the Chaya Career Advancement Chair, the Russel Berrie Nanotechnology Institute, and the Grand Technion Energy Program, and G.G. and N. Aho were supported by the Academy of Finland (Grant 311031).

1. Mulkidjanian AY, Heberle J, Cherepanov DA (2006) Protons @ interfaces: Implications for biological energy conversion. *Biochim Biophys Acta* 1757:913–930.
2. Williams RJP (1988) Proton circuits in biological energy interconversions. *Annu Rev Biophys Biophys Chem* 17:71–97.
3. Agmon N (1995) The Grotthuss mechanism. *Chem Phys Lett* 244:456–462.
4. Knight C, Voth GA (2012) The curious case of the hydrated proton. *Acc Chem Res* 45: 101–109.
5. Öjemyr LN, Lee HJ, Gennis RB, Brzezinski P (2010) Functional interactions between membrane-bound transporters and membranes. *Proc Natl Acad Sci USA* 107: 15763–15767.
6. Alexiev U, Mollaaghababa R, Scherrer P, Khorana HG, Heyn MP (1995) Rapid long-range proton diffusion along the surface of the purple membrane and delayed proton transfer into the bulk. *Proc Natl Acad Sci USA* 92:372–376.
7. Gopta OA, Cherepanov DA, Junge W, Mulkidjanian AY (1999) Proton transfer from the bulk to the bound ubiquinone Q(B) of the reaction center in chromatophores of Rhodobacter sphaeroides: Retarded conveyance by neutral water. *Proc Natl Acad Sci USA* 96:13159–13164.
8. Heberle J, Riesle J, Thiedemann G, Oesterhelt D, Dencher NA (1994) Proton migration along the membrane surface and retarded surface to bulk transfer. *Nature* 370:379–382.
9. Lechner RE, Dencher NA, Fitter J, Dippel T (1994) Two-dimensional proton diffusion on purple membrane. *Solid State Ion* 70:296–304.
10. Teissié J, Prats M, Soucaille P, Tocanne JF (1985) Evidence for conduction of protons along the interface between water and a polar lipid monolayer. *Proc Natl Acad Sci USA* 82:3217–3221.
11. Springer A, Hagen V, Cherepanov DA, Antonenko YN, Pohl P (2011) Protons migrate along interfacial water without significant contributions from jumps between ionizable groups on the membrane surface. *Proc Natl Acad Sci USA* 108:14461–14466.
12. Zhang C, et al. (2012) Water at hydrophobic interfaces delays proton surface-to-bulk transfer and provides a pathway for lateral proton diffusion. *Proc Natl Acad Sci USA* 109:9744–9749.

13. Weichselbaum E, et al. (2017) Origin of proton affinity to membrane/water interfaces. *Sci Rep* 7:4553.
14. Serowy S, et al. (2003) Structural proton diffusion along lipid bilayers. *Biophys J* 84: 1031–1037.
15. Sandén T, Salomonsson L, Brzezinski P, Widengren J (2010) Surface-coupled proton exchange of a membrane-bound proton acceptor. *Proc Natl Acad Sci USA* 107: 4129–4134.
16. Brändén M, Sandén T, Brzezinski P, Widengren J (2006) Localized proton microcircuits at the biological membrane-water interface. *Proc Natl Acad Sci USA* 103:19766–19770.
17. Wolf MG, Grubmüller H, Groenhof G (2014) Anomalous surface diffusion of protons on lipid membranes. *Biophys J* 107:76–87.
18. Medvedev ES, Stuchebrukhov AA (2013) Mechanism of long-range proton translocation along biological membranes. *FEBS Lett* 587:345–349.
19. Yamashita T, Voth GA (2010) Properties of hydrated excess protons near phospholipid bilayers. *J Phys Chem B* 114:592–603.
20. Re S, Nishima W, Tahara T, Sugita Y (2014) Mosaic of water orientation structures at a neutral zwitterionic lipid/water interface revealed by molecular dynamics simulations. *J Phys Chem Lett* 5:4343–4348.
21. Medvedev ES, Stuchebrukhov AA (2011) Proton diffusion along biological membranes. *J Phys Condens Matter* 23:234103.
22. Toppozini L, et al. (2015) Anomalous and anisotropic nanoscale diffusion of hydration water molecules in fluid lipid membranes. *Soft Matter* 11:8354–8371.
23. Antonenko YN, Pohl P (2008) Microinjection in combination with microfluorimetry to study proton diffusion along phospholipid membranes. *Eur Biophys J* 37:865–870.
24. Åkerman J (2005) Applied physics. Toward a universal memory. *Science* 308:508–510.
25. Nachliel E, Gutman M (1988) Time-resolved proton-phospholipid interaction. Methodology and kinetic analysis. *J Am Chem Soc* 110:2629–2635.
26. Amdursky N, Simkovitch R, Huppert D (2014) Excited-state proton transfer of photoacids adsorbed on biomaterials. *J Phys Chem B* 118:13859–13869.
27. Pines E, Huppert D, Agmon N (1988) Geminate recombination in excited-state proton-transfer reactions: Numerical solution of the Debye–Smoluchowski equation with backreaction and comparison with experimental results. *J Chem Phys* 88:5620–5630.
28. Amdursky N (2015) Photoacids as a new fluorescence tool for tracking structural transitions of proteins: Following the concentration-induced transition of bovine serum albumin. *Phys Chem Chem Phys* 17:32023–32032.
29. Cohen B, Álvarez CM, Carmona NA, Organero JA, Douhal A (2011) Proton-transfer reaction dynamics within the human serum albumin protein. *J Phys Chem B* 115: 7637–7647.
30. Awasthi AA, Singh PK (2017) Excited-state proton transfer on the surface of a therapeutic protein, protamine. *J Phys Chem B* 121:10306–10317.
31. Simkovitch R, Huppert D (2015) Excited-state proton transfer of weak photoacids adsorbed on biomaterials: Proton transfer to glucosamine of chitosan. *J Phys Chem A* 119:641–651.
32. Simkovitch R, Huppert D (2015) Excited-state proton transfer of weak photoacids adsorbed on biomaterials: 8-hydroxy-1,3,6-pyrenetrisulfonate on chitin and cellulose. *J Phys Chem A* 119:1973–1982.
33. Agmon N (2005) Elementary steps in excited-state proton transfer. *J Phys Chem A* 109: 13–35.
34. Agmon N, Pines E, Huppert D (1988) Geminate recombination in proton-transfer reactions. II. Comparison of diffusional and kinetic schemes. *J Chem Phys* 88: 5631–5638.
35. Huppert D, Goldberg SY, Masad A, Agmon N (1992) Experimental determination of the long-time behavior in reversible binary chemical reactions. *Phys Rev Lett* 68: 3932–3935.
36. Cherepanov DA, Feniouk BA, Junge W, Mulkidjanian AY (2003) Low dielectric permittivity of water at the membrane interface: Effect on the energy coupling mechanism in biological membranes. *Biophys J* 85:1307–1316.
37. Teschke O, Ceotto G, de Souza EF (2001) Interfacial water dielectric-permittivity-profile measurements using atomic force microscopy. *Phys Rev E Stat Nonlin Soft Matter Phys* 64:011605.
38. Finkler B, et al. (2014) Highly photostable "super"-photoacids for ultrasensitive fluorescence spectroscopy. *Photochem Photobiol Sci* 13:548–562.
39. Spies C, et al. (2014) Solvent dependence of excited-state proton transfer from pyranine-derived photoacids. *Phys Chem Chem Phys* 16:9104–9114.
40. Barnadas-Rodríguez R, Estelrich J (2008) Effect of salts on the excited state of pyranine as determined by steady-state fluorescence. *J Photochem Photobiol Chem* 198: 262–267.
41. Pines E, Fleming GR (1991) Proton transfer in mixed water-organic solvent solutions: Correlation between rate, equilibrium constant, and the proton free energy of transfer. *J Phys Chem* 95:10448–10457.
42. Jacquemin D, Perpète EA, Ciofini I, Adamo C (2008) Fast and reliable theoretical determination of pKa* for photoacids. *J Phys Chem A* 112:794–796.
43. Pines D, Pines E (2007) Solvent assisted photoacidity. *Hydrogen-Transfer Reactions* (Wiley-VCH, Weinheim, Germany), pp 377–415.
44. Krissinel EB, Agmon N (1996) Spherical symmetric diffusion problem. *J Comput Chem* 17:1085–1098.
45. Amdursky N, Rashid MH, Stevens MM, Yarovsky I (2017) Exploring the binding sites and proton diffusion on insulin amyloid fibril surfaces by naphthol-based photoacid fluorescence and molecular simulations. *Sci Rep* 7:6245.
46. Agmon N, Gutman M (2011) Bioenergetics: Proton fronts on membranes. *Nat Chem* 3: 840–842.
47. Medvedev ES, Stuchebrukhov AA (2006) Kinetics of proton diffusion in the regimes of fast and slow exchange between the membrane surface and the bulk solution. *J Math Biol* 52:209–234.
48. Amdursky N, Orbach R, Gazit E, Huppert D (2009) Probing the inner cavities of hydrogels by proton diffusion. *J Phys Chem C* 113:19500–19505.